Supplementary Information

List of figures :

Figure S1. Percent of values above the MDL for each element measured with the Xact.

Figure S2. (a) Changes in $\Delta Q/Q_{exp}$, ΔUEV_{real} and ΔUEV_{noisy} for n-(n+1)-factor PMF_{metals} runs and **(b)** Q/Q_{exp}, UEV_{real} and UEV_{noisy} for PMF_{metals} runs from 1 to 8 factors. These PMF runs are performed for the WFP dataset. The box plots located in the blue dashed-line area represent the values for the finalized 6-factors bootstrap solution using the total metals dataset.

Figure S3. Factors time series (left) and profiles (right) from the PMF solution using the FDP dataset. The regional background factor profile was constrained with an a-value of 0.1.

Figure S4. Criteria scores for the 100 bootstrapped runs from the PMF_{metals}. Each graph represents one criterion for the different factors. The blue markers are for the factor criterion scores and the black markers represent the second highest scores attributed to one of the remaining factors.

Figure S5. (a) NO_x, SO_2 and O_3 concentration and **(b)** wind speed and direction during OP measurement period.

Figure S6. (a) Comparison between time series of PM_1 measured by FIDAS and time series of particulate fraction reconstituted by the sum of chemical components ($r_s = 0.47$, $p < 0.001$). **(b)** Contribution to PM_1 of chemical components (%) measured from 11th July 2018 to 25th July 2018 (included firework episode, n=91) by ToF-ACSM, Xact and aethalometer online analyzers.

Figure S7. (a) Average mass spectra profiles, **(b)** time-series, **(c)** pie chart contributions and **(d)** mean diurnal cycles (solid lines and error bars indicate the standard deviation) for the 5 factors from the $PMF_{organics}$ solution.

Figure S8. (a) Pie chart contributions and **(b)** average diurnal profiles of factors from the PMF_{metals} analysis. For the diurnal plots the red dots correspond to the mean, the bands are the median, the bottom and top of the boxes represent the 25th and 75th percentile respectively, and the ends of the whiskers are for the 10th and 90th percentiles.

Figure S9. NWR plots for the different factors from the PMF_{metals} analysis.

Figure S10. Probability density function of scaled residuals for the standalone ACSM_OA, ACSM, AE33 and Xact datasets.

Figure S11. Box plots of dust resuspension factor concentrations for different relative humidity (RH) bins in %. The concentrations are enhanced under low RH conditions. The blue diamonds are the mean, the bars inside the boxes the median, the bottom and top of the boxes are the 25th and 75th percentile, respectively, and the ends of the whiskers are the 10th and 90th percentiles.

Figure S12. Criteria scores for the a-values sensitivity test runs from the PMF_{PM1}. Each graph represents one criterion per factor. The grey markers are the unselected runs, the blue markers are the selected runs for the related factor and the green markers are the effectively chosen runs.

Figure S13. Number of accepted solutions based on the PMF_{PM1} criteria list for the different a-values explored in the sensitivity test. A-values associated to the greatest number of validated solutions were

chosen for the bootstrap PMF runs (i.e. 0.4 for biomass burning, 0.1 for cooking and 0.05 for industrial constrained profiles).

Figure S14. Relative contributions of PM_1 factors profiles and unexplained variations from the PMF_{PM1} analysis.

Figure S15. Comparison between the industrial metals profile from our study and ICP-MS profiles for the $PM_{2.5}$ fraction in the industrial area of Fos-sur-mer (Sylvestre et al., 2017). Complex n°1 is a cast iron converter complex, complex n°2 is a ore iron converter complex, complex n°3 is a blast furnace slag storage and complex n°4 is an ore terminal.

Figure S16. Average diurnal profiles for SO_2, Sh-IndOA and the sum of industrial and shipping factors from the PMF_{metals}.

Figure S17. Residuals values of WLS models for **(a)** OP_{AA} and **(b)** OP_{DTT}. An outlier point (07/19/2018 03:00) was withdrawn to ensure homoscedasticity of residuals values.

Figure S18. Mean contribution of the sources identified by PMF_{PM1} over the OP sampling campaign (n = 86) to **(a)** OP_{AA}, **(b)** OP_{DTT}, **(c)** PM_1. Error bars represents the standard deviation of the data distribution.

List of tables :

Table S1. List of elements measured with the Xact, their respective MDLs and the percent of measurements above the MDL.

Table S2. Summary of statistics for the different PMF tests carried out on the WFP datasets of metals. 18 downweight conditions were tested for the PMF inputs. The matrix including a S2N downweight and errors below MDLs downweighted with $\alpha_i = 2 \times r_{P95}$ (test n°12) was selected as final inputs.

Table S3. Intrinsic OP_{AA} and OP_{DTT} (OP_m) provided by weighted robust linear regression with an M-estimator expressed in $nmol.min^{-1}.\mu g^{-1}$ of sources provided by **(a)** $PMF_{organics}$ (scenario 1) and **(b)** PMF_{metals} (scenario 2) over the OP sampling campaign (n = 90). Values are the mean ± standard deviation from bootstraps runs for both OP assays. The model parameters $R^2_{adjusted}$ and Pearson's correlation between model OP and observed OP are mentioned on the right.

Table S4. Factors identification for the PMF_{PM1} analyses between 5 and 12 factors. The green cells represent the base case identification for the related factors. The remaining undefined factors for each solution corresponded to mixed profiles not attributed to a specific source. The red squares are the base cases used as reference profile constraints.

Table S5. Pearson's correlation coefficients between OP_{vAA} and OP_{vDTT} to the PM sources identified by PMF_{PM1} model.

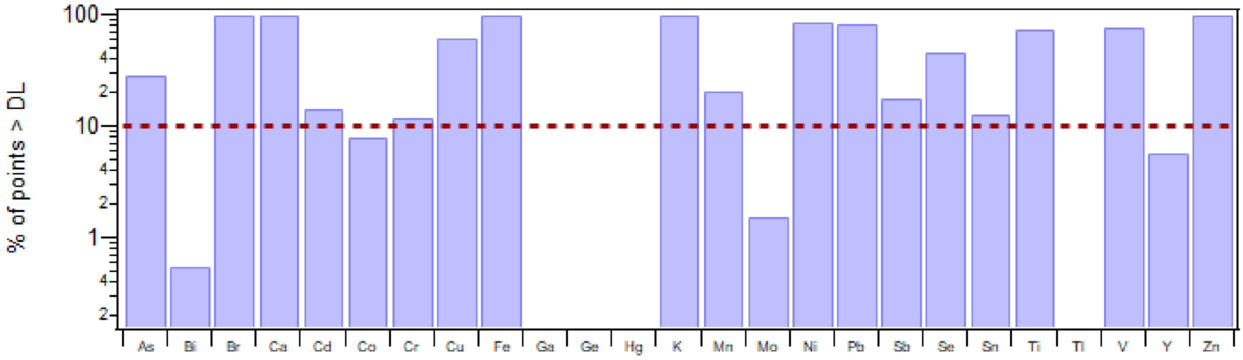

Figure S1. Percent of values above the MDL for each element measured with the Xact.

Elements	MDL ($ng.m^{-3}$)	Values > MDL (%)
As	0.11	**29.3**
Bi	0.23	**0.6**
Br	0.18	**99.8**
Ca	0.52	**99.5**
Cd	4.4	**14.4**
Co	0.24	**8.1**
Cr	0.2	**12.0**
Cu	0.14	**63.3**
Fe	0.3	**100**
Ga	0.1	0
Ge	0.1	0
Hg	0.21	0.2
K	2	**100**
Mn	0.25	**20.6**
Mo	0.84	1.5
Ni	0.17	**86.6**
Pb	0.22	**84.8**
Sb	9	**18.0**
Se	0.14	**46.4**
Sn	7.1	**12.8**
Ti	0.28	**76.0**
Tl	0.2	0
V	0.21	**76.7**
Y	0.48	5.8
Zn	0.12	**100**

Table S1. List of elements measured with the Xact, their respective MDLs and the percent of measurements above the MDL.

Error matrix downweights for PMF_{metals}

Polissar et al. (1998) (Polissar et al., 1998a) first introduced an uncertainty of 5/6 × MDL for data below MDL (set to MDL/2). The purpose was to provide relative errors for these values 2 to 5 times greater than the maximum relative errors of the data exceeding the MDLs. Here, several uncertainties values were tested for data below MDL by conducted a panel of PMF runs with 2 to 8 factors. The errors were calculated by applying a downweight coefficient (α) to the previous formula from Polissar et al. (1998) (Polissar et al., 1998a):

$$\sigma_{i,j} = \alpha \times \frac{5}{6} MDL_i \text{ if } x_{i,j} < MDL_i \quad \text{(S1)}$$

For all the elements i, α was set to 6, 10 and 14 in order to obtain a ratio of 2, 3.5 and 5, respectively, with the maximum relative error found in the dataset, i.e. 476% for Sn (the value corresponds to the 95th percentile instead of the max value to avoid outlier effects). Another test consisted in applying a dependant α based on the maximum relative error (95th percentile) for each element i (r_{P95}):

$$\alpha_i = 2 \times r_{P95} \quad \text{(S2)}$$

Where 2 was used to determine the same ratio between the relative error of data below the MDLs from Polissar et al. (1998) equation (167 %, considering the $\frac{5}{6}MDL/\frac{1}{2}MDL$ calculation) and the maximum relative error for the data greater than the MDLs (50%) found in Polissar et al. (1998) (Polissar et al., 1998a) dataset. A last test was performed with α=1 (i.e. no downweight) for the comparison. Each PMF analysis was also conducted with and without 1/S2N downweight (Visser et al., 2015). The tests were performed on the WFP dataset and the results were synthetized in Table S2. Here we focus on the 5F-solutions results as they resolved unmixed factors and represented a statistically relevant number of factor (see section 2.4.2 in the main text).

For all PMF solutions, applying the 1/S2N downweight provided lower scaled residuals as shown by the narrower width of fits. The solutions with α=1 (i.e. no errors downweight for data <MDLs) were discarded due to less satisfactory mass reconstructions and residuals and higher average unexplained variations. The unexplained variation is a dimensionless quantity which indicates how much variation (in time or in each variable) is not explained by the factors (Canonaco et al., 2013). Thus, the unexplained variation of the i^{th} point for the factor k^{th} is:

$$UEV_{ik} = \frac{\sum_{j=1}^{m}(|e_{ij}|/\sigma_{ij})}{\sum_{j=1}^{m}((\sum_{k=1}^{p}|g_{ik} \cdot f_{kj}| + e_{ij})/\sigma_{ij})} \quad \text{(S3)}$$

UEV is further calculated for data with S2N>2 (UEV_{real}) or for noisy data (UEV_{noisy}).

The remaining tests gave comparable explained variations, mass reconstitutions and residuals. The uncertainties calculated with $\alpha_i = 2 \times r_{P95}$ (test n°12 in Table S2) were finally selected as error inputs for the data below the MDLs since this solutions resolved 5 unmixed factors with the best mean and median diurnal patterns for each identified source.

Tests	**N°**	**Unexplained Variations**			**$\Sigma_{factors}$ vs Σ_{metals}**		**Sc residuals**	
		F5 EV_Noise	F5 EV_Real	F5 EV_Sum	F5 Slope	F5 R^2	F5 center	F5 width
noDW_noS2N	**1**	0.215	0.049	0.264	0.987	0.958	0.094	0.337
noDW_S2N	**2**	0.221	0.042	0.263	0.987	0.959	0.059	0.201
DW6_ALL_noS2N	**3**	0.187	0.048	0.235	0.989	0.973	-0.023	0.137
DW6_ALL_S2N	**4**	0.203	0.033	0.236	1.004	0.985	-0.002	0.014
DW6_SPEC_noS2N	**5**	0.187	0.041	0.228	1.000	0.979	-0.010	0.089
DW6_SPEC_S2N	**6**	0.203	0.033	0.236	1.003	0.986	-0.002	0.014
DW10_ALL_noS2N	**7**	0.187	0.040	0.227	1.010	0.993	-0.020	0.074
DW10_ALL_S2N	**8**	0.201	0.033	0.234	1.015	1.000	-0.002	0.005
DW10_SPEC_noS2N	**9**	0.187	0.040	0.227	1.010	0.993	-0.020	0.073
DW10_SPEC_S2N	**10**	0.201	0.033	0.234	1.014	1.000	-0.002	0.005
Roll_DW_ALL_noS2N	**11**	0.188	0.041	0.229	1.007	0.988	-0.013	0.091
Roll_DW_ALL_S2N	**12**	0.203	0.034	0.237	1.010	0.995	-0.001	0.005
Roll_DW_SPEC_noS2N	**13**	0.187	0.041	0.228	1.006	0.988	-0.013	0.091
Roll_DW_SPEC_S2N	**14**	0.203	0.034	0.237	1.011	0.995	-0.002	0.011
DW14_ALL_noS2N	**15**	0.189	0.040	0.229	1.016	1.000	-0.023	0.063
DW14_ALL_S2N	**16**	0.204	0.032	0.236	1.017	0.999	-0.002	0.005
DW14_SPEC_noS2N	**17**	0.189	0.040	0.229	1.016	1.000	-0.023	0.063
DW14_SPEC_S2N	**18**	0.203	0.033	0.236	1.023	1.000	-0.001	0.003

Table S2. Summary of statistics for the different PMF tests carried out on the WFP datasets of metals. 18 downweight conditions were tested for the PMF inputs. The matrix including a S2N downweight and errors below MDLs downweighted with $\alpha_i = 2 \times r_{P95}$ (test n°12) was selected as final inputs.

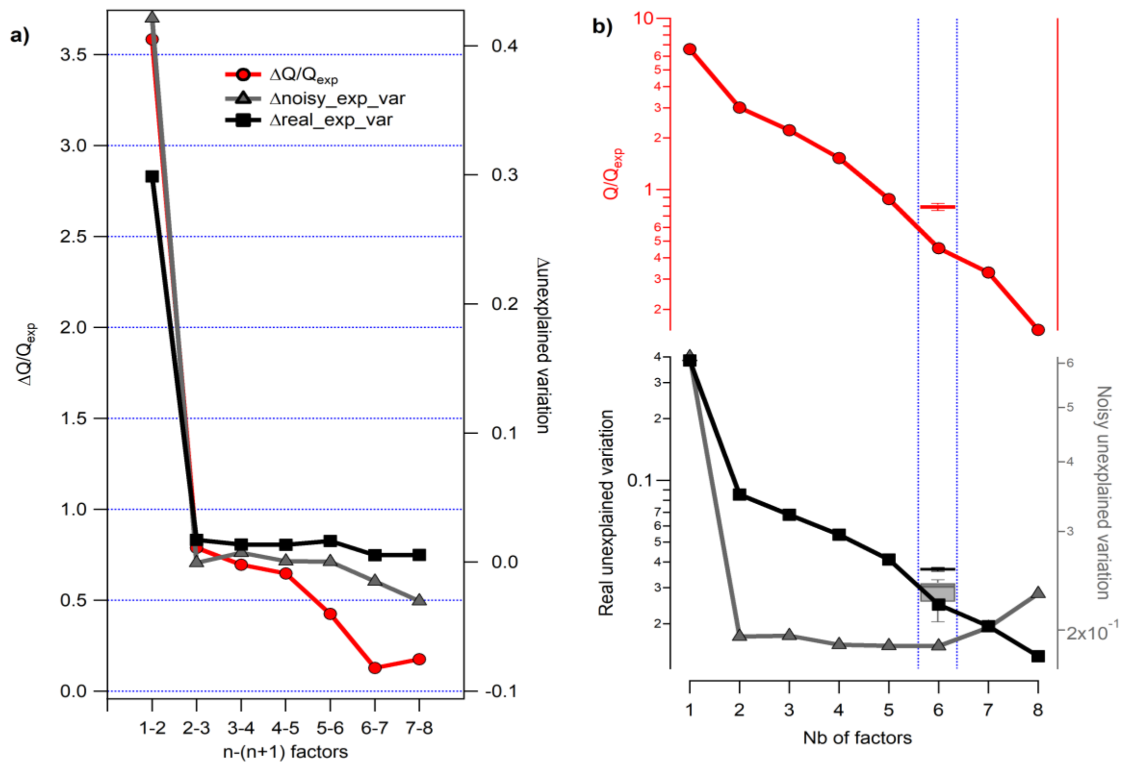

Figure S2. **(a)** Changes in $\Delta Q/Q_{exp}$, ΔUEV_{real} and ΔUEV_{noisy} for n-(n+1)-factor PMF_{metals} runs and **(b)** Q/Q_{exp}, UEV_{real} and UEV_{noisy} for PMF_{metals} runs from 1 to 8 factors. These PMF runs are performed for the WFP dataset. The box plots located in the blue dashed-line area represent the values for the finalized 6-factors bootstrap solution using the total metals dataset.

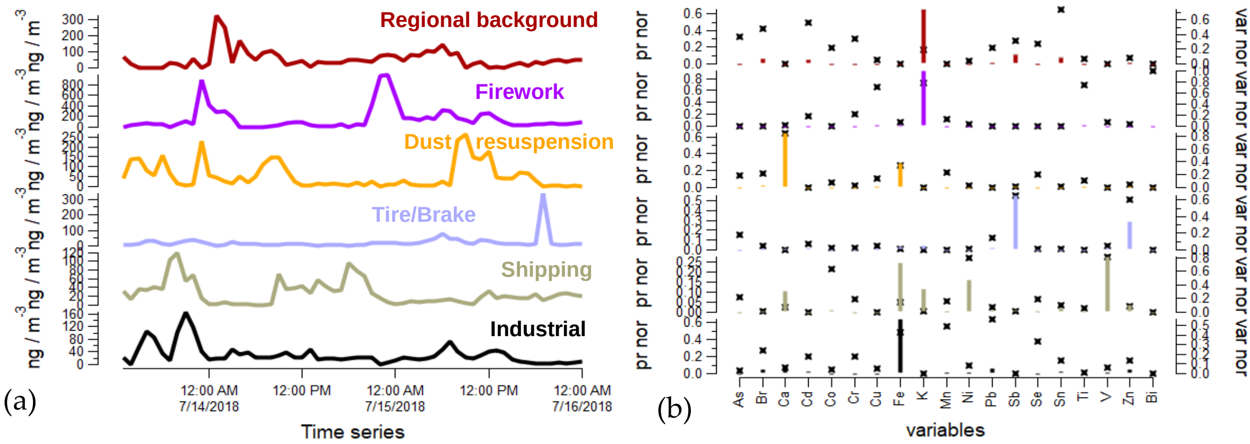

Figure S3. (a) Factors time series and **(b)** profiles from the PMF solution using the FDP dataset. The regional background factor profile was constrained with an a-value of 0.1.

Criteria selection for PMF_{metals}

A first type of criterion was the use of the dominant element in the related factor. Thus, the Bi, Ca, Zn, V and Fe intensity in profiles were monitored for the Firework, Dust resuspension, Tire/brake wear, Shipping and Industrial factors, respectively. Then we inspected the r Pearson correlation with MOOA for the regional background. A last criterion was the r Pearson correlation based on the multilinear regression analysis of both shipping and industrial vs SO_2 concentrations. The statistical acceptance of a run was based on the comparison between the criterion scores of a factor and the second highest scores from the remaining factors (Fig. S4). For all criteria the second highest scores were much lower in every run, with some rejected scores for the firework criterion. In total 25% of the runs were discarded based on this criterion, and the remaining runs were averaged into a unique solution.

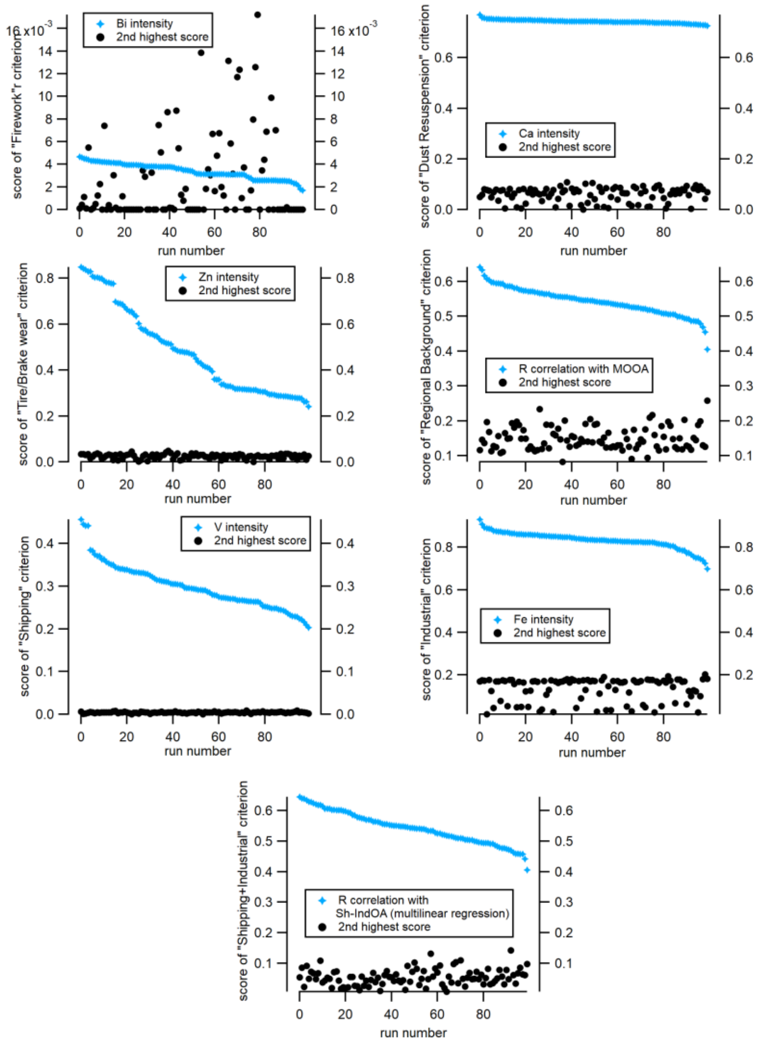

Figure S4. Criteria scores for the 100 bootstrapped runs from the PMF_{metals}. Each graph represents one criterion for the different factors. The blue markers are for the factor criterion scores and the black markers represent the second highest scores attributed to one of the remaining factors.

Scenario and regression model selection for OP apportionment

Three scenarii in the construction of the matrix of the source factors contribution to PM mass identified by the three PMF have been considered to make the best use of the results from the different PMF:

- Scenario 1: OP apportionment from independent variables with the OA factors from $PMF_{organics}$ (83 observations), following:

$$OP = G \times \beta_g + \varepsilon \tag{S4}$$

- Scenario 2: OP apportionment from independent variables considering only the metals factors from PMF_{metals} (90 observations), following:

$$OP = H \times \beta_h + \varepsilon \tag{S5}$$

- Scenario 3: OP apportionment taking as independent variables PM_1 factors from PMF_{PM1} (78 observations), following (Eq. S6). In this configuration, the firework episode has been removed from the data as the sources from the PMF_{PM1} analysis have been determined without including the firework metal factor.

$$OP = I \times \beta_i + \varepsilon \tag{S6}$$

In (Eq. S4, S5, S6), OP vector (px1) is the observed OP expressed in volume unit, *G* matrix (g x (p+1)) of *g* sources (plus the intercept) is determined by $PMF_{organics}$, H matrix (h x (p+1)) of *h* sources (plus the intercept) is determined by PMF_{metal}, I matrix (i x (p+1)) of *i* sources (plus the intercept) is determined by PMF_{PM1}, and ε vector (px1) is the discrepancy between the model and the observations.

Three models were tested for the three scenarii (e.g. 9 solutions): weighted least squares linear regression (WLS), weighted robust multiple linear regression with an iterative M-estimator, and partial least square regression (PLS):

- WLS regression considers the uncertainties σ of the OP measurements by minimizing the weighted sum of squares function (WSS):

$$WSS\ (\beta) = \sum_{i=1}^{p} w_i \left(y_i - \sum_{j=1}^{n} x_{ij} * \beta_j\right)^2,\ w_i = \frac{1}{\sigma_i} \tag{S7}$$

where y_i is the measured OP (p observations), x_{ij} is the values of n sources determined by PMF and σ_i is the OP uncertainties. This method already used in this purpose in previous studies (Borlaza et al., 2021; Weber et al., 2018, 2021) well suited to extracting maximum information from small data sets. Ordinary Least Squares (OLS) is a simple special case of WLS where σ = 1.

- Linear weighted robust regression methods by M-estimator minimizes the function ϱ:

$$M\ (\beta) = \sum_{i=1}^{p} \rho(w_i\ (y_i\ \sum_{j=1}^{n} x_{ij} * \beta_j)) \tag{S8}$$

$$\rho_k(x) = \begin{cases} \frac{x^2}{2} & if\ |x| < k = 1.5 \\ k\left(|x| - \frac{k}{2}\right) & if\ |x] \geq\ k = 1.5 \end{cases} \qquad \text{(S9)}$$

Based on similar work in Grange et al. (2022), Huber's function ϱ and k=1.5 were used in this study. This technique is adapted to data sets presenting particular events(de Menezes et al., 2021), as fireworks on 13th and 14th of July -National day of France- in our data set. Indeed, the regression by successive iterations implies lower weights on outliers, which tends to underestimate these points. We can note WLS regression is a simple special case where $\varrho(x) = x^2$.

- PLS regression is a method that reduces the predictors to a smaller set of uncorrelated components and performs least squares regression on these components. It is especially useful when dependent variables are highly correlated. Moreover, unlike multiple regression, PLS does not imply that the predictors are fixed but can be measured with error, making PLS more robust to measurement uncertainties.

OP apportionment from $PMF_{organics}$ (scenario 1) and PMF_{metals} (scenario 2)

M-estimator inversion model's results issued from $PMF_{organics}$ (scenario 1) and PMF_{metals} (scenario 2) alone are respectively presented in Table S 3a. and Table S 3b. β coefficients (i.e intrinsic OP, see 2.5) obtained by M-estimator model from PMF_{metals} display values an order of magnitude higher than those issued from $PMF_{organics}$ inversion. This stress the importance of metals in OP apportionment, for both assays. Among the organic factors, only the Sh-IndOA factor seems to be slightly more sensitive to OP_{vDTT}. The Firework factor constrains a significant part of the data, implying a fairly high Pearson's correlation coefficient between OP_{model} and $OP_{observed}$. Nevertheless, $R^2_{adjusted}$ of both M-estimator inversion models in scenario 1 (only organic fraction of PM is considered) indicated that the percentage of OP_{AA} and OP_{DTT} variance explained by the models is weak. On the other hand, several studies highlighted the role of Secondary Organic Aerosol (SOA) in the oxidative potential indicating that apportion OP from the metallic data alone is an incomplete step. Finally, the bootstrap method (see 2.5) applied to the four M-estimator models in these two scenarii did not achieve their convergence and are therefore not robust. Overall, this confirms that OP reflects the overall redox-activity of wide spectra of multispecies of organics, inorganics, metals and synergistic/antagonistic reactions between these compounds, and assess the importance to consider all these chemical compounds in the OP apportionment process.

(a)

	Intercept	COA	HOA	LOOA	MOOA	Sh-IndOA	R^2 ajusted	r ($OP_{observed}/OP_{model}$)
OP_{AA}	0.19 ± 0.04	0.00 ± 0.02	0.02 ± 0.01	0.10 ± 0.04	0.04 ± 0.02	0.24 ± 0.09	0.27	0.48***
OP_{DTT}	0.38 ± 0.10	-0.04 ± 0.10	-0.12 ± 0.05	0.23 ± 0.04	0.1 ± 0.07	1.41 ± 0.15	0.41	0.51***

(b)

	Intercept	Firework	Industrial	Regional background	Shipping	Tire brake	R^2 ajusted	r ($OP_{observed}/OP_{model}$)
OP_{AA}	0.36 ± 0.02	1.57 ± 0.16	3.21 ± 0.42	2.30 ± 0.33	-0.74 ± 0.68	n.c.	0.66	0.73***
OP_{DTT}	0.61 ± 0.12	4.17 ± 0.83	-1.24 ± 1.64	7.11 ± 2.30	17.0 ± 5.3	6.0 ± 4.60	0.38	0.61***

Table S3. Intrinsic OP_{AA} and OP_{DTT} (OP_m) provided by weighted robust linear regression with an M-estimator expressed in nmol.min^{-1}.µg^{-1} of sources provided by **(a)** $PMF_{organics}$ (scenario 1) and **(b)** PMF_{metals} (scenario 2) over the OP sampling campaign (n = 90). Values are the mean ± standard deviation from bootstraps runs for both OP assays. The model parameters $R^2_{adjusted}$ and Pearson's correlation between model OP and observed OP are mentioned on the right.

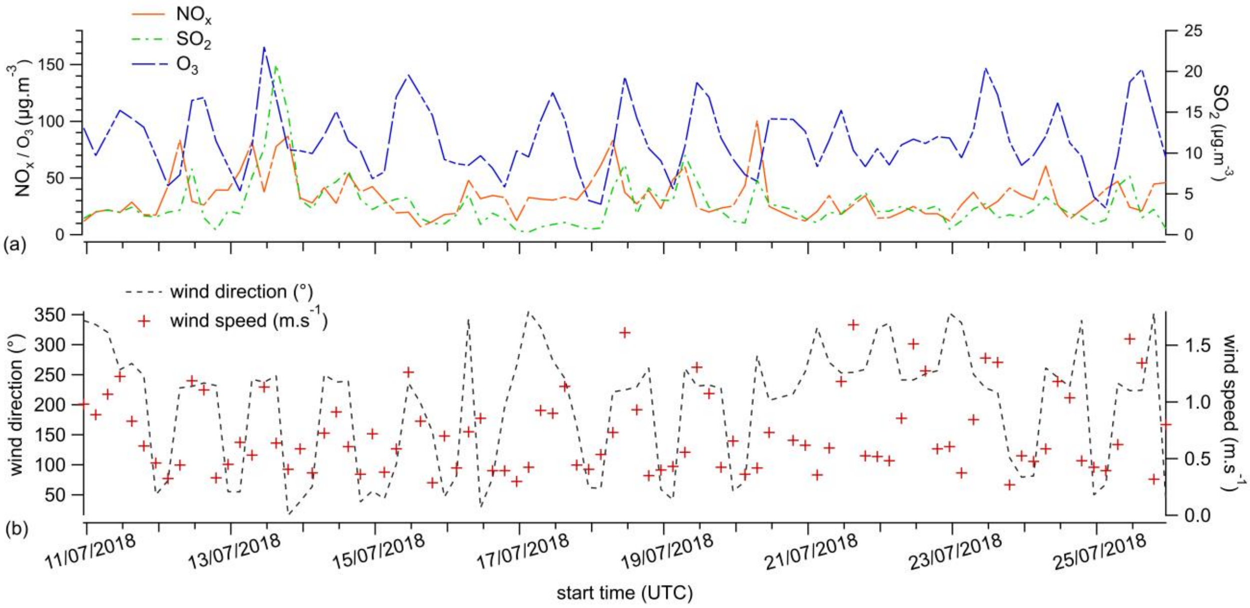

Figure S5. (a) NO_x, SO_2 and O_3 concentration and **(b)** wind speed and direction during OP measurement period.

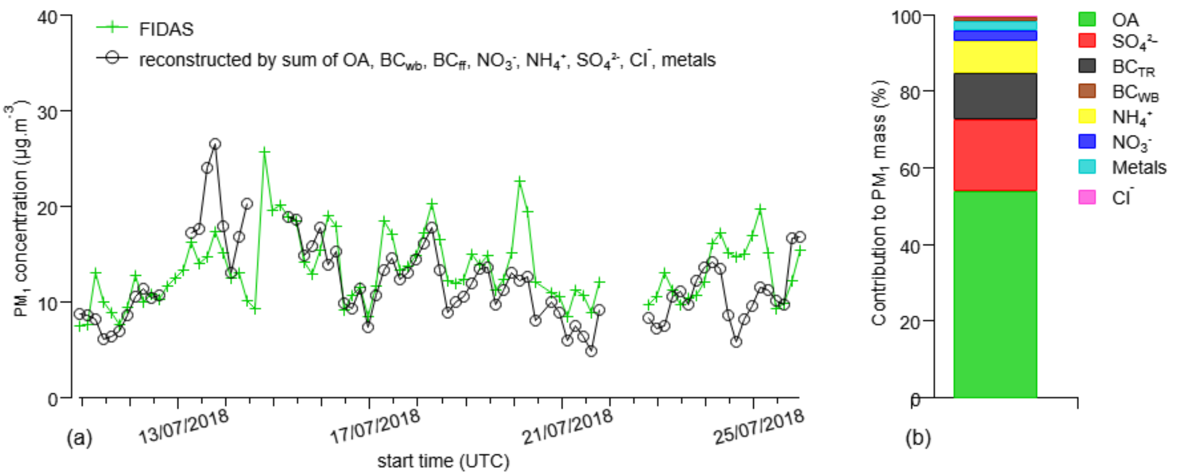

Figure S6. (a) Comparison between time series of PM_1 measured by FIDAS and time series of particulate fraction reconstituted by the sum of chemical components ($r_s = 0.47$, $p < 0.001$); **(b)** Contribution to PM_1 of chemical components (%) measured from 11th July 2018 to 25th July 2018 (included firework episode, n=91) by ToF-ACSM, Xact and aethalometer online analyzers.

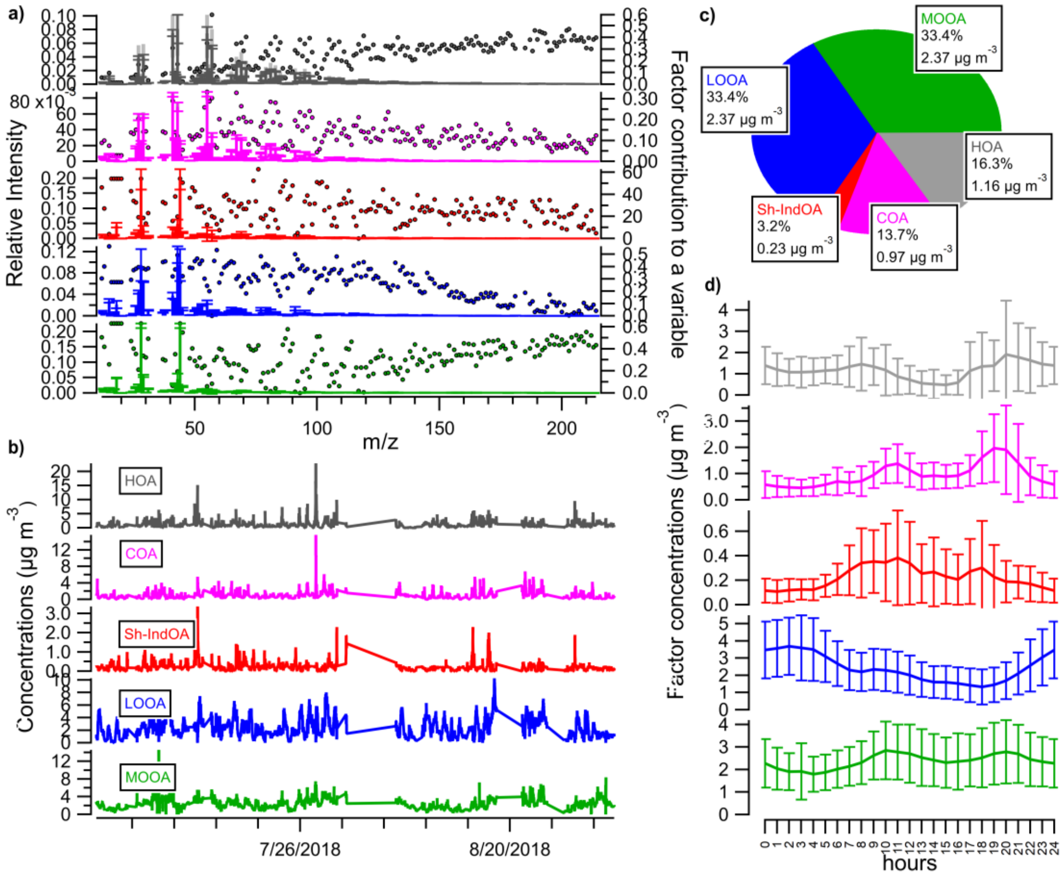

Figure S7. **(a)** Average mass spectra profiles, **(b)** time-series, **(c)** pie chart contributions and **(d)** mean diurnal cycles (solid lines and error bars indicate the standard deviation) for the 5 factors from the $PMF_{organics}$ solution.

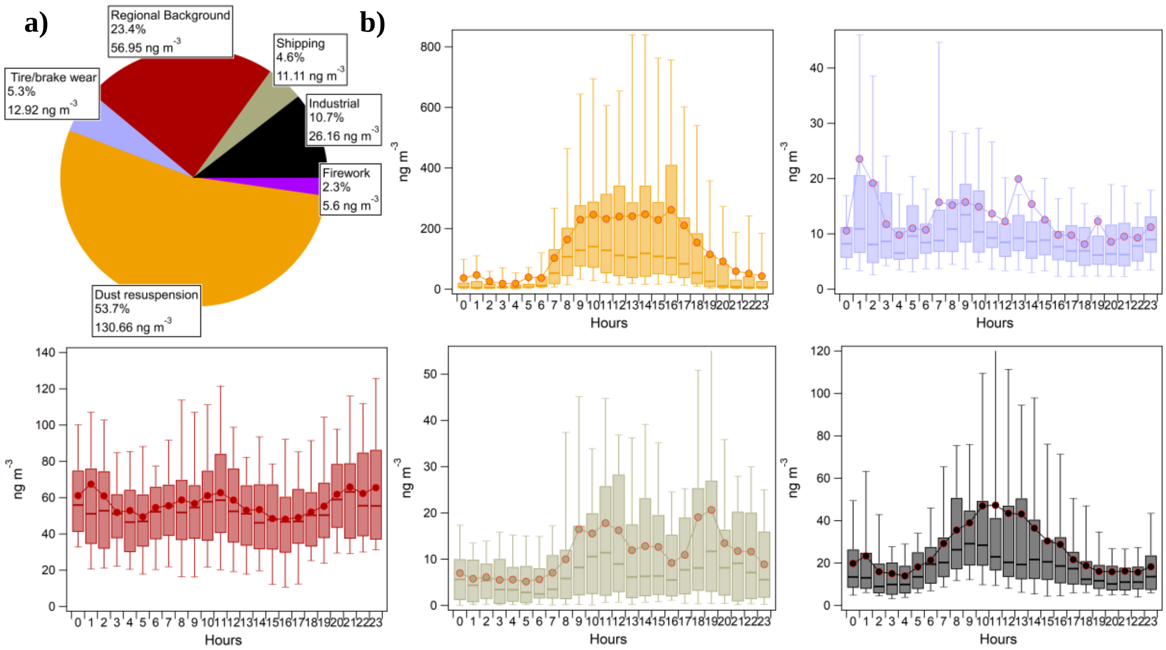

Figure S8. (a) Pie chart contributions and **(b)** average diurnal profiles of factors from the PMF_{metals} analysis. For the diurnal plots the red dots correspond to the mean, the bands are the median, the bottom and top of the boxes represent the 25^{th} and 75^{th} percentile respectively, and the ends of the whiskers are for the 10^{th} and 90^{th} percentiles.

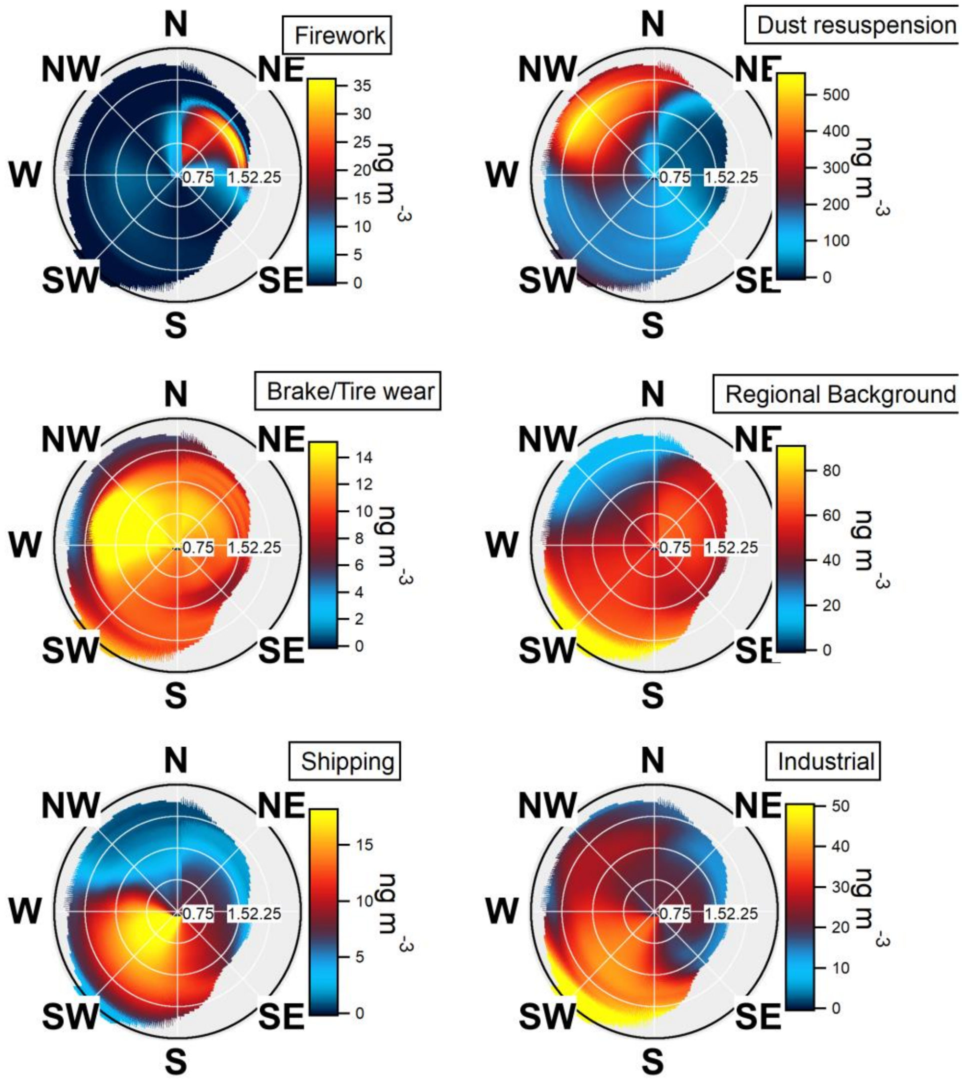

Figure S9. NWR plots for the different factors from the PMF_{metals} analysis.

C-value weighting

The instrument weight was controlled by applying a scaling factor (i.e. C-value) to the uncertainties of each group of components (Slowik et al., 2010):

$$(\sigma'_{i,j})_s = \frac{(\sigma_{i,j})_s}{C_s} \tag{S10}$$

σ represents the uncertainties, C the scaling value applied to the s datasets. Here we distinguished the $PMF_{organics}$ (*ACSM_OA*), PMF_{metals} (*Xact*), ACSM inorganics (*ACSM*) and BC (*AE33*) datasets. A well balanced solution should show magnitude of scaled residuals independent from the instrument. Since their scaled residuals were rather in the same range, a C-value of 1 was chosen for ACSM_OA, Xact and ACSM datasets and resulted in unweighted results. However, we applied a C-value of 5 to the AE33 dataset, meaning that dataset of BC concentrations were upweighted. The overlapping of scaled residuals from the different instrument datasets is shown in Figure .

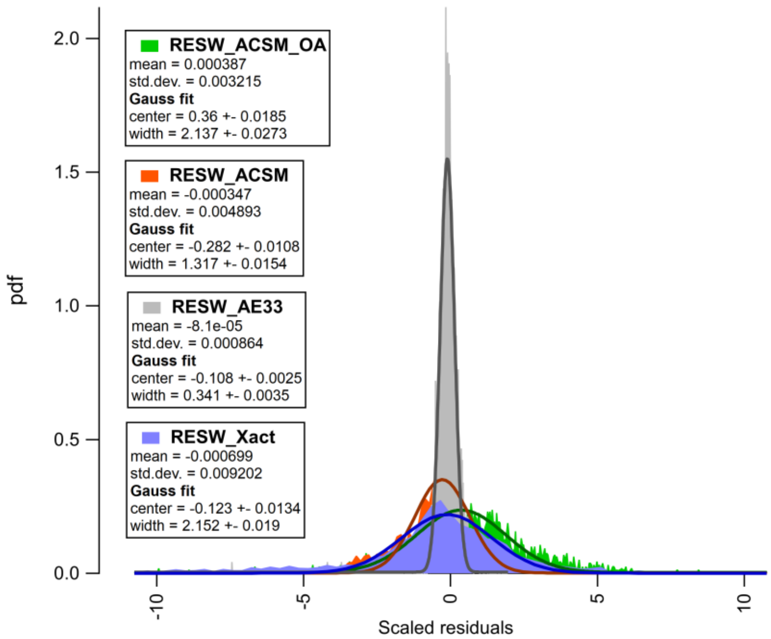

Figure S10. Probability density function of scaled residuals for the standalone ACSM_OA, ACSM, AE33 and Xact datasets.

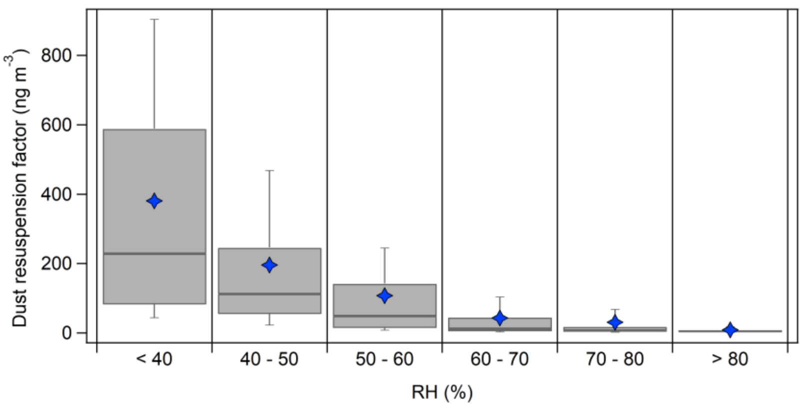

Figure S11. Box plots of dust resuspension factor concentrations for different relative humidity (RH) bins in %. The concentrations are enhanced under low RH conditions. The blue diamonds are the mean, the bars inside the boxes the median, the bottom and top of the boxes are the 25th and 75th percentile, respectively, and the ends of the whiskers are the 10th and 90th percentiles.

Factors identification and rotational ambiguity exploration for PMF_{PM1}

Seed runs between 1 and 12 factors were examined. The factors interpretability was based on profiles consistency and our expectations from the factors composition. The summarizes the occurrence of 8 well-identified factors in all runs between 5 and 12 factors. The choice of a 8-factors solution is supported also by mathematical diagnostics ($\Delta Q/Q_{exp}$, , mass reconstruction, ΔUEV – not presented here) which showed that realistic solutions can be found up to 5 factors. While some factors are easily resolved in most of the solutions (e.g. dust resuspension) some others are retrieved from an elevated number of factor (e.g. shipping and cooking are found in up to 9 factors-solution).

Therefore, the solution was constrained using base case profiles (Table). The biomass burning, cooking and industrial factors were constrained as they presented unstable profiles across the different runs. Constraining the industrial factor allow an improved separation of the shipping factor (see the discussion below).

	5F	6F	7F	8F	9F	10F	11F	12F
Traffic								
Dust								
AS-rich								
ON-rich								
Industrial								
Shipping								
BB								
Cooking								

Table S4. Factors identification for the PMF_{PM1} analyses between 5 and 12 factors. The green cells represent the base case identification for the related factors. The remaining undefined factors for each solution corresponded to mixed profiles not attributed to a specific source. The red squares are the base cases used as reference profile constraints.

To inspect the best combination of a-values for the profile constraints, we performed a-values sensitivity analyses by scanning a-values from 0 to 0.5 with increment of 0.05, leading to 1330 outcomes. The goodness of the solutions was examined with a criteria selection list and the scores are presented in the Figure . First, the R^2 correlations between biomass burning, cooking and industrial factors with their corresponding constraint were monitored. Then, we monitored the intensity of the dominant variable in the related factor profiles: $Dust_{metals}$ for dust resuspension, BC_{FF} for traffic, LOOA for ON-rich, SO_4^{2-} for AS-rich and Sh-IndOA for shipping. Sh-IndOA was inspected instead of $shipping_{metals}$ to ensure a clear separation between shipping and industrial factors since Sh-IndOA is assumed to only be attributed to these two factors. For the first seven criteria, the scores were much higher than the second highest scores (not displayed in the graph). Therefore, some runs were only discarded based on the shipping criterion as we only selected the runs whose Sh-IndOA intensity was in the same range than the base case profile from the preliminary analyses. Moreover, the selected runs (green markers in Figure) showed similar scores intensity for traffic, ON-rich, AS-rich and dust resuspension than those found in their respective base case profile. In the end, the same criteria list was used for the bootstrap runs selection.

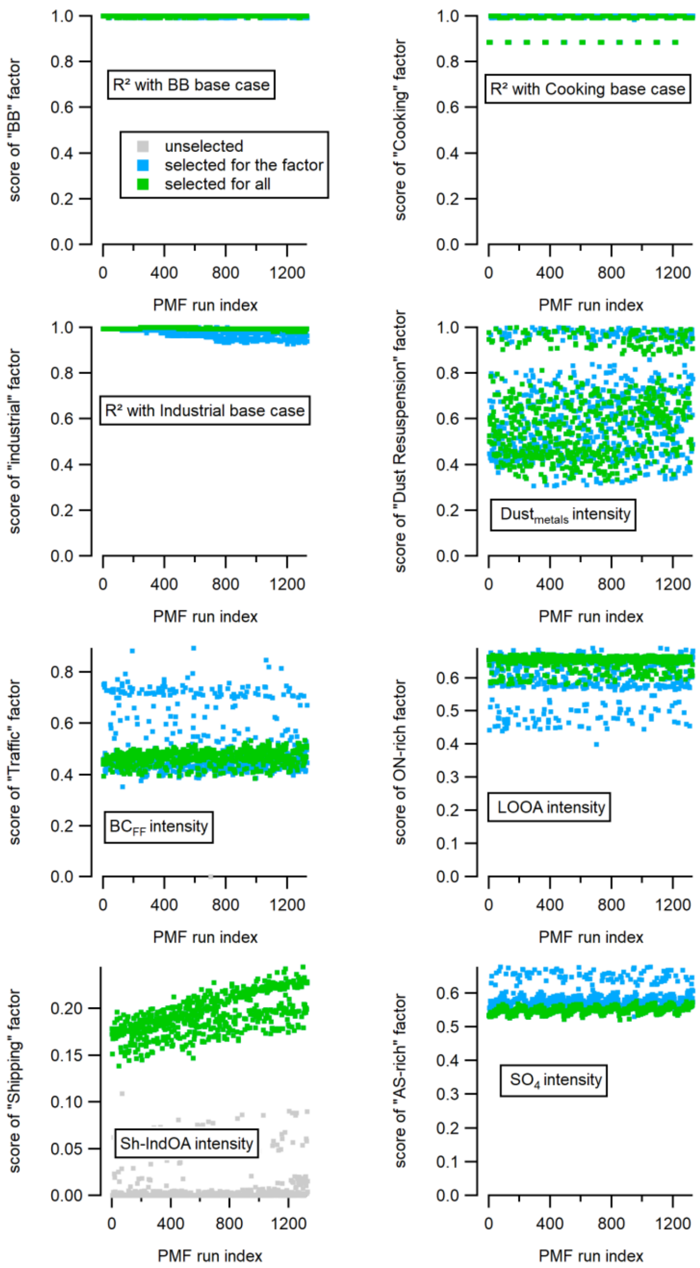

Figure S12. Criteria scores for the a-values sensitivity test runs from the PMF_{PM1}. Each graph represents one criterion per factor. The grey markers are the unselected runs, the blue markers are the selected runs for the related factor and the green markers are the effectively chosen runs.

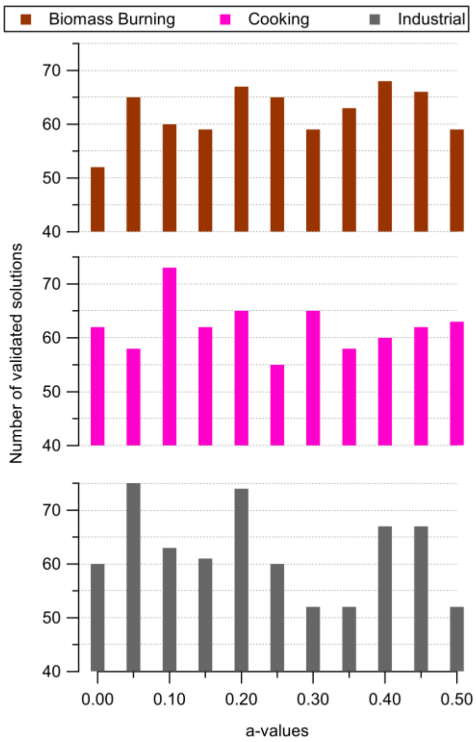

Figure S13. Number of accepted solutions based on the PMF_{PM1} criteria list for the different a-values explored in the sensitivity test. A-values associated to the greatest number of validated solutions were chosen for the bootstrap PMF runs (i.e. 0.4 for biomass burning, 0.1 for cooking and 0.05 for industrial constrained profiles).

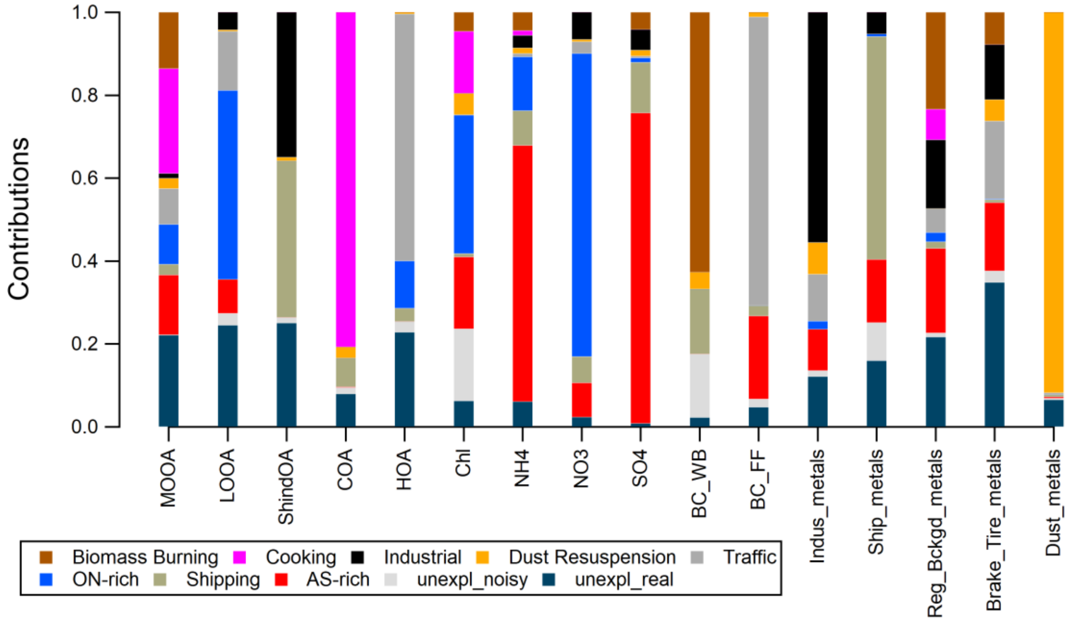

Figure S14. Relative contributions of PM_1 factors profiles and unexplained variations from the PMF_{PM1} analysis.

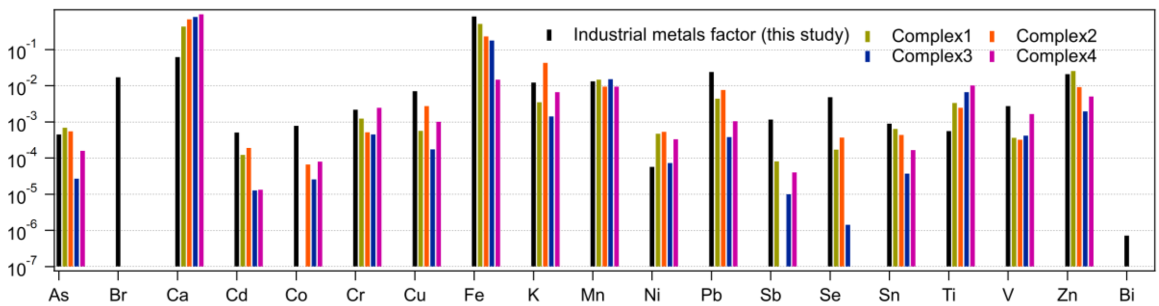

Figure S15. Comparison between the industrial metals profile from our study and ICP-MS profiles for the $PM_{2.5}$ fraction in the industrial area of Fos-sur-mer (Sylvestre et al., 2017). Complex n°1 is a cast iron converter complex, complex n°2 is a ore iron converter complex, complex n°3 is a blast furnace slag storage and complex n°4 is an ore terminal.

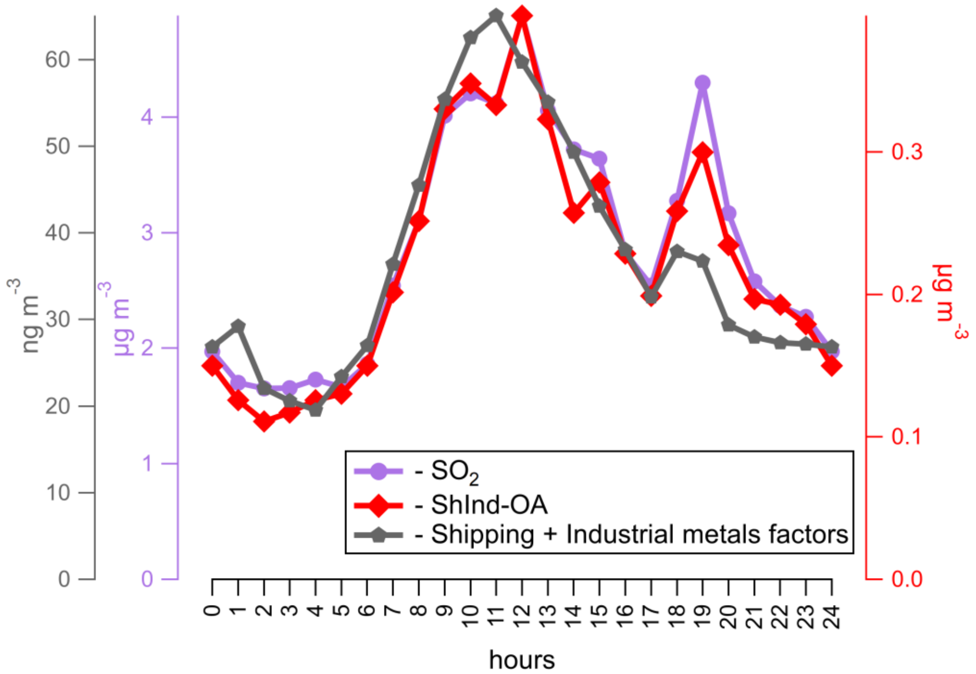

Figure S16. Average diurnal profiles for SO_2, Sh-IndOA and the sum of industrial and shipping factors from the PMF_{metals}.

Associations between both OP and sources of PM

Pearson's correlation coefficients (r) between the source factor contributions identified by the PMF_{PM1} and both OP assays are presented in Table with the idea to provide a first estimate of the associated sources with OP. We note that no source strongly correlates alone to both OP assays, but moderate correlations (0.3< r<0.5) can be noted for both OP vs. Traffic source (OP_{vAA}: r=0.40, p<0.001 - OP_{vDTT}: r=0.34, p<0.01) and Shipping source (OP_{vAA}: r=0.32 - OP_{vDTT}: r=0.30, p<0.01). OP_{vAA} also correlates moderately with Industrial source (r=0.41, p<0.001) and ON-rich source (r=0.32, p<0.01). Finally, OP_{vDTT} displays a mild correlation with AS-rich source (r=0.36, p<0.01), but this correlation might be attributed to a collinearity with PM mass (r OP_{vDTT} vs SO_4^{2-}=0.46, r OP_{vDTT} vs NH_4^+ = 0.47 - p<0.001).

	Biomass Burning	**Cooking**	**Industrial**	**Dust resuspension**	**Traffic**	**ON-rich**	**Shipping**	**AS-rich**
$OP_{v\,AA}$	0.15	0.18	0.41***	0.13	0.40***	0.32***	0.32**	0.17
$OP_{v\,DTT}$	0.12	-0.02	0.14	0.14	0.34**	0.19	0.30	0.36**

***p < 0.001, **p < 0.01

Table S5. Pearson's correlation coefficients between OP_{vAA} and OP_{vDTT} to the PM sources identified by PMF_{PM1} model**.**

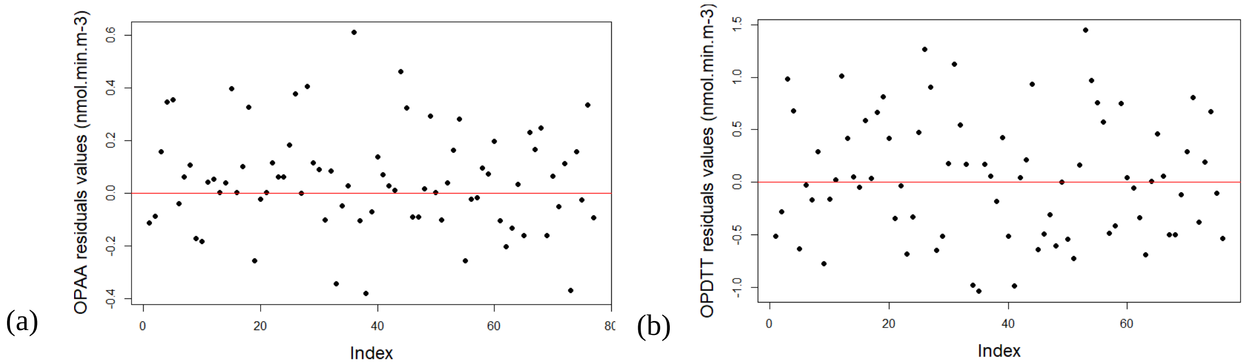

Figure S17. Residuals values of WLS models for **(a)** OP_{AA} and **(b)** OP_{DTT}. An outlier point (19 July 2018 03:00) was withdrawn to ensure homoscedasticity of residuals values.

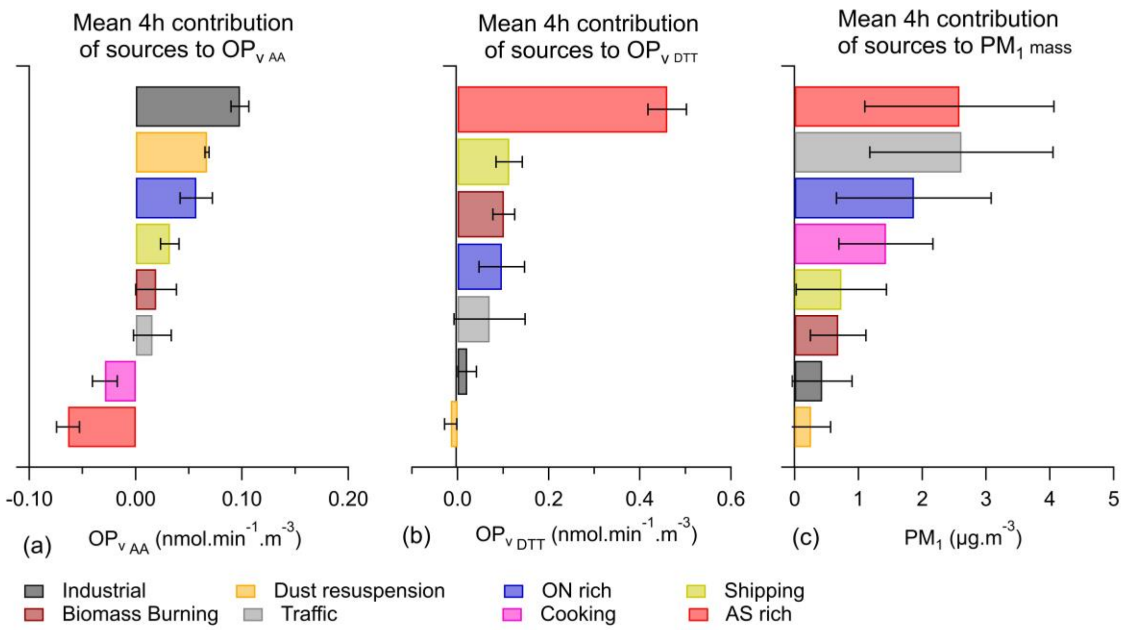

Figure S18. Mean contribution of the sources identified by PMF_{PM1} over the OP sampling campaign (n = 86) to **(a)** OP_{AA}, **(b)** OP_{DTT}, **(c)** PM_1. Error bars represents the standard deviation of the data distribution.